Effect of silica aerosil particles on liquid-crystal phase transitions

Hisashi Haga and Carl W. Garland
School of Science and Center for Material Science and Engineering, Massachusetts Institute of Technology, Cambridge, Massachusetts 02139
(Received 28 April 1997)

High-resolution ac calorimetric studies show that the dispersion of 70-Å-diameter hydrophilic silica spheres (aerosils) has a substantial effect on several liquid-crystal transitions in butyloxybenzlidene octylaniline (4O.8). The weakly first-order nematic (N)–isotropic (I), the second-order nematic (N)–smectic-A (SmA), and the strongly first-order smectic-A(SmA)–crystal-B(CrB) freezing transition all exhibit shifted transition temperatures and substantial changes in the shape of excess heat capacity peaks. Power-law fits show an evolution of the N–SmA critical exponent α from $\alpha=0.135$ in bulk 4O.8 toward $\alpha\approx\alpha_{XY}=-0.007$ in 4O.8+aerosil suspensions with silica densities $\rho_s\approx 0.08$ g cm^{-3}. For $\rho_s\geqslant 0.11$ g cm^{-3}, the N–SmA ΔC_p peaks are rounded in a manner qualitatively like those for 4O.8 confined in a high-porosity aerogel, one of which was also studied. [S1063-651X(97)04009-9]

PACS number(s): 61.30.−v, 64.70.Md, 82.70.Rr.

I. INTRODUCTION

The effects of quenched randomness on critical phase transition behavior is an active field of research. Much of this work has been carried out on magnetic systems [1], but studies of a liquid crystal (LC) confined in aerogels [2–7] and porous glasses [8–9] have been vigorously pursued over the past five years. See Ref. [10] for a general review of such liquid-crystal studies.

A recent calorimetric study has been made of the nematic (N)–smectic-A (SmA) transition in octylcyanobiphenyl (8CB) with small aerosil particles (70-Å SiO_2 particles) suspended in it [11]. This work showed that such 8CB+aerosil systems with silica densities $\rho_s=0.016-0.167$ g cm^{-3} were consistent with earlier 8CB +aerogel results on systems with $\rho(\text{gel})=0.08-0.60$ g cm^{-3} [5]. Indeed, the shifts in $T_c(N-\text{Sm}A)$ for both types of system exhibit the same dependence on ρ, and the same is true for the integrated enthalpies $\delta H(N-\text{Sm}A)$. More importantly, 8CB+aerosil samples with $\rho_s\lesssim 0.09$ g cm^{-3} exhibit singular $\Delta C_p(N-\text{Sm}A)$ excess heat-capacity peaks that can be power-law analyzed to obtain the heat-capacity critical exponent α_{eff}. The resulting α_{eff} values decrease monotonically from $\alpha=0.30\pm 0.02$ for pure bulk 8CB to $\alpha\approx -0.03$ for $\rho\approx 0.09$ g cm^{-3}. The latter value is very close to the theoretical value for a three-dimensional (3D) XY model, $\alpha_{XY}=-0.007$ [12]. This model is expected to describe the N–SmA transition, and does so for the heat capacity of bulk liquid crystals in which the coupling between the smectic order parameter and the orientational nematic order parameter is weak [13].

The present paper extends the work in Ref. [11] in two ways: a preparation method has been developed for suspending sil particles more uniformly than can be achieved with mechanical stirring, and the present liquid crystal N-(4-n-butyloxybenzlidene-4′-n-octylaniline) (4O.8) is a nonpolar LC with a monomeric SmA_m phase instead of the ''frustrated'' polar compound 8CB with a partial bilayer SmA_d phase. The preparation technique has allowed us to prepare 4O.8+aerosil samples with ρ_s as large as 0.438 g cm^{-3}. In addition, we studied 4O.8 in one aerogel ($\rho=0.25$ g cm^{-3}). Thus we can compare the present C_p results with a detailed frequency-dependence study of $\Delta C_p(\omega,T)$ for 4O.8+aerogel samples [6] as well as with previous studies of 8CB in aerogels and 8CB with suspended aerosils [5,11]. It should be noted that very recent SAXS (small-angle x-ray-scattering) data show that aerosils suspended in a LC exhibit structures [14] which are very similar to those of aerogels [5].

The compound 4O.8 ($M=365.56$ g mol^{-1}) has the structural formula

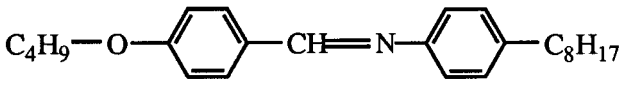

and exhibits the phase sequence

$$\underset{}{\text{Cr}K} \underset{311.2\text{ K}}{\text{——}} \text{Cr}B \underset{\sim 322.6\text{ K}}{\text{——}} \text{Sm}A \underset{336.9\text{ K}}{\text{——}} N \underset{352\text{ K}}{\text{——}} I,$$

where the transition temperatures are taken from Refs. [15–17]. There are two 3D crystal phases—the rigid crystal K(CrK), which is the stable phase at room temperature, and the plastic crystal B(CrB); I denotes the isotropic phase. Thus it is possible to explore the effect of aerosil particles on the second-order N–SmA transition, the weakly first-order N-I transition, and the strongly first-order SmA–CrB transition. The terms weak and strong first order refer to the relative size of the latent heat ΔH compared with the integrated C_p pretransitional enthalpy $\delta H=\int\Delta C_p dT$ ($\Delta H\leqslant\delta H$ is weak and $\Delta H\gg\delta H$ is strong).

There is still a paucity of theory appropriate to the description of either LC+aerogel or LC+aerosil systems. Two types of simple theoretical models—single-pore and random-field Ising—are reviewed briefly in Ref. [11]. Our aim is to stimulate new theory and new experiments with other techniques. Experimental work on LC+aerosil systems is attrac-

tive since they are much easier to prepare than LC+aerogel systems. Section II gives our experimental procedures and reports the effects of several aerosil densities and one aerogel sample on the N-I, $N-\mathrm{Sm}A$, and $\mathrm{Sm}A-\mathrm{Cr}B$ transitions. Section III presents the excess ΔC_p associated with the phase transitions, and gives a power-law analysis of the $N-\mathrm{Sm}A$ sil data. A general discussion of the effects of aerosils and aerogels on the N-I and $\mathrm{Sm}A-\mathrm{Cr}B$ first-order transitions as well as the continuous $N-\mathrm{Sm}A$ transition is given in Sec. IV.

II. EXPERIMENTAL PROCEDURES AND RESULTS

The 4O.8 sample used in the present work was provided by J. D. Litster, and was originally synthesized by Organix Corporation. It had a melting point of 311.5 K and was used without further purification. For most experiments, a hydrophilic aerosil (type 300) was used as obtained from Degussa Corporation [18] without further processing. This sil consists of 70-Å-diameter SiO_2 spheres, with hydroxyl groups covering the surface. The surface area is given by the manufacturer as 300 $m^2\ g^{-1}$, and the particle size distribution is fairly narrow (full width at half maximum of distribution $\sim$75 Å) [18]. One sil dispersion was made with a hydrophobic (type R812) aerosil with CH_3 surface groups.

The LC+aerosil samples were prepared by dissolving the LC in pure absolute ethanol ($\sim$0.02-g LC per cm^3 of solvent), adding the aerosil powder, and then sonicating for $\sim$1 h to achieve a good dispersion. The solvent was evaporated off slowly ($\sim$15 h) at 60 °C. The sample was then placed in a vacuum system at 10^{-3} Torr and pumped on for one day at $\sim$90 °C. The resulting density ρ_s denotes the grams of SiO_2 per cm^3 of liquid crystal. Note that if no LC is used, the aerosil that remains after evaporation of the solvent forms a very fragile 3D ''structure'' of density $\sim$0.13 g cm^{-3} that is much like a high porosity aerogel.

The $\rho=0.25$ g cm^{-3} silica aerogel was prepared at Massachusetts Institute of Technology (MIT) in the same manner as the aerogels described in Ref. [5]. Although not investigated by SAXS, its characteristic parameters can be estimated quite well by interpolation from data available on four aerogels with densities in the range 0.08–0.60 g cm^{-3} [5]. Such aerogels have fractal network structures with strut dimensions of about 100 Å, and average solid chord lengths $d_s \approx 47$ Å. For the $\rho=0.25$ gel, we estimate an average pore chord L of 280 ± 60 Å and a pore volume fraction ϕ_p of 0.86. The density ρ_s defined above can be obtained from $\rho_s=\rho(\mathrm{gel})/\phi_p$, which yields $\rho_s \simeq 0.29$ g/cm^3 LC for this aerogel. The essential aspect of preparing a 4O.8+aerogel sample is to avoid having 4O.8 freeze into the rigid CrK phase at any time since this will significantly damage the fragile aerogel network [6,19].

The filling of the aerogel with 4O.8 was accomplished with a procedure which differed from that used previously [5–7], and which was designed to minimize damage to the fragile gel. A thin slab of empty aerogel was placed in the cup of a shallow ($\sim$1 mm deep) silver cell. The cell and aerogel were heated so that 4O.8 placed on the top surface of the gel would melt and go into the isotropic phase. As a low viscosity isotropic liquid, 4O.8 is drawn into the pores of the gel by capillary action. More 4O.8 is added in small amounts as needed until the gel is full, as determined visually. The cell is then weighed and cold-weld sealed without any handling of the gel slab. Once sealed and mounted in the calorimeter, the cell is maintained at or above the bulk freezing temperature. Fortunately, cycling of the sample through the $\mathrm{Sm}A-\mathrm{Cr}B$ transition has no effect on the data [6].

After a 4O.8 or 4O.8+aerosil sample was prepared, it was cold-weld sealed into a silver cell $\sim$1 cm in diameter and $\sim$1 mm thick. For bulk 4O.8, a helix of gold wire was also included to enhance the internal thermal conductivity [20]. No gold wire was used for 4O.8+aerosil samples. In this case, the fact that the thermal conductivity of SiO_2 is seven times greater than that of a typical liquid crystal should somewhat speed up heat flow in the sample and help to reduce or eliminate internal temperature gradients.

The high-resolution ac calorimetric technique is ideal for studying phase transitions (especially second order ones) in small samples, and descriptions of this method are given elsewhere [20]. Explicit details for the calorimeter used in this work are given in Ref. [21], together with the equations for processing the observed T_{ac} response to a $P_{\mathrm{ac}}\exp(i\omega t)$ heat input. The standard frequency $\omega_o=0.196\ \mathrm{s}^{-1}$ (corresponding to a 32-s period or frequency $f=\omega_o/2\pi$ of 31.25 mHz) used here for bulk 4O.8, and the philic aerosil samples is that used in most previous work at MIT. The essential equations in the absence of two-phase coexistence are

$$C_p=[C'_{\mathrm{filled}}(T)-C_{\mathrm{empty}}]/m, \tag{1}$$

$$C''_{\mathrm{filled}}=\frac{|P_{\mathrm{ac}}|}{\omega|T_{\mathrm{ac}}|}\sin\phi-\frac{1}{\omega R}, \tag{2}$$

where C_{empty} is the heat capacity of the empty silver cell (plus gold in the case of bulk runs) and m is the mass of the liquid crystal in grams. $C'_{\mathrm{filled}}=(|P_{\mathrm{ac}}|/\omega|T_{\mathrm{ac}}|)\cos\phi$ and C''_{filled} are the real and imaginary components of the heat capacity of a cell containing a sample. The quantity R is the thermal resistance between sample and bath, and $\phi\equiv\Theta+\pi/2$, where Θ is the shift in the phase of T_{ac} with respect to that of P_{ac} [6,21]. All data were obtained on cooling, and scan rates of about -50 mK/h were used. It can be shown that C_p measured in a one-phase region for 4O.8+philic aerosils at the standard frequency ω_o correspond to static C_p values. For 4O.8+aerogels it is known that $C_p(\omega_o)<C_p$ (static) [6], and the aerogel was studied at $\omega_o/2$, as was the one 4O.8+phobic aerosil sample. The phase transition temperatures were very stable; the drifts were less than 1 mK over $\sim$7 days of data acquisitions for a given sample.

The heat capacity of pure bulk 4O.8 is shown in Fig. 1. Data points obtained in a two-phase coexistence region exhibit anomalously large ϕ values and apparent C_p values that are artificially high due to qualitative latent heat effects [20]. Such points are denoted by $\times$ in Fig. 1. For cooling scans, we observed a two-phase N-I coexistence region 270 mK wide and centered at 352.08 K, a second-order $C_p(N-\mathrm{Sm}A)$ singularity at 336.924 K, and a two-phase $\mathrm{Sm}A-\mathrm{Cr}B$ coexistence region 680 mK wide and centered at 322.37 K (an abrupt jump in C_p occurred at 322.71 K on cooling). These values agree well with all the previous literature [6,15–17] except that the T_{NI} value reported in Ref. [6] is $\sim$1.0 K too high, and the T_{AB} value given in Ref. [16a] is $\sim$0.4 K higher

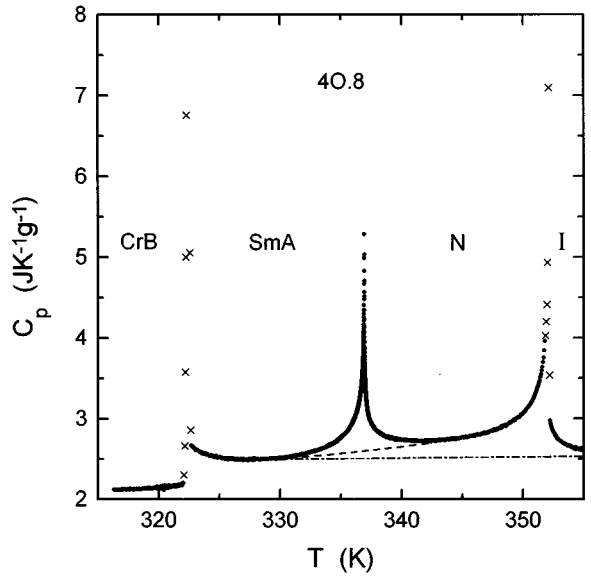

FIG. 1. Heat capacity of bulk 4O.8. Points indicated with a cross ($\times$) are artificial C_p values obtained in two-phase coexistence regions. The dashed line represents the C_p(background) curve used in Eq. (3) to determine the excess heat capacity ΔC_p associated with the $N-$SmA transition. The dashed dot line is C_p(background) for obtaining $\Delta C_p(N\text{-}I)$.

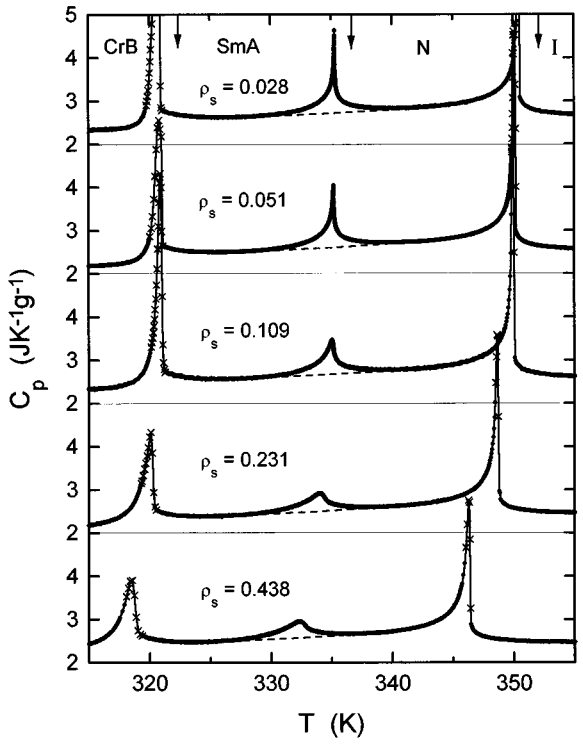

FIG. 2. Heat capacity C_p for five 4O.8+philic aerosil samples with the silica densities ρ_s in g cm^{-3} indicated. See the legend of Fig. 1 for the meaning of $\times$ points and the dashed lines. The arrows at the top margin indicate the positions of the transitions of bulk 4O.8 obtained in Fig. 1.

than the present value. The overall $C_p(T)$ behavior in Fig. 1 agrees well with that given in Refs. [16] and [17], and $C''_{\text{filled}}=0$ was observed except in two-phase coexistence regions.

The heat capacity $C_p(T)$ is shown in Fig. 2 over a wide temperature range for five 4O.8+philic aerosil systems with silica densities ρ_s from 0.028 to 0.438 g cm^{-3}. Again the symbol $\times$ marks points in a two-phase coexistence region. The phase shift ϕ is shown in Fig. 3 for the $\rho_s=0.109$ system as a typical example of 4O.8+aerosil behavior. The dips in ϕ at the $N-$SmA transition and in the wings of the N-I and Sm$A-$CrB transitions are a direct consequence of the C_p peaks in one-phase regions and lead to $C''_{\text{filled}}=0$ as expected for static one-phase data. The anomalous large values of ϕ that signal two-phase coexistence at first-order transitions [5,22] are clearly visible at the N-I and Sm$A-$CrB transitions. Further corroboration of the first-order character of these two 4O.8+aerosil transitions was provided by a nonadiabatic scanning run (linear-ramp relaxation method [21]) on the $\rho_s=0.438$ sample. This technique measures enthalpy changes and detects the total transition enthalpy $\Delta H+\delta H$, where ΔH is the first-order latent heat. The total enthalpy exceeded δH(ac) by 1.12 J g^{-1} for the N-I transition, and 2.13 J g^{-1} for the Sm$A-$CrB transition. There was no difference in the $N-$SmA enthalpy determined with ac calorimetry and nonadiabatic scanning calorimetry, as expected for a continuous transition where $\Delta H=0$.

It is clear from Fig. 2 that there are substantial shifts in the transition temperatures even for very low aerosil concentrations. In order to verify that these are due to LC aerosil interactions rather than any impurity effects, the following experiment was carried out. A 4O.8+aerosil sample was prepared in the usual manner and ''aged'' for 2.5 days by cycling the temperature between 320 and 355 K. This sample was then centrifuged at 6000 rpm for 1 h at 60 °C (in the SmA phase) in order to separate the 4O.8 and the aerosil particles. The recovered 4O.8 was degassed in the N phase for one day, and the transition temperatures determined microscopically, agreed very well with those for the bulk 4O.8

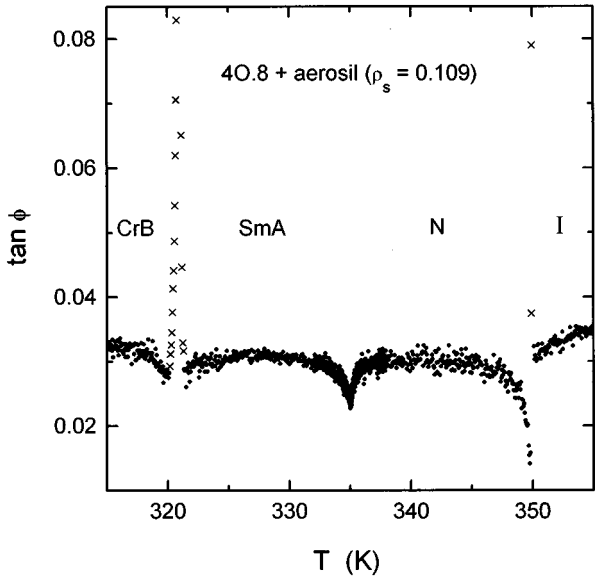

FIG. 3. Phase shift ϕ of the 4O.8+philic aerosil sample with $\rho_s=0.109$ g cm^{-3}. The sharp peaks indicated by $\times$ symbols are in regions of two-phase coexistence.

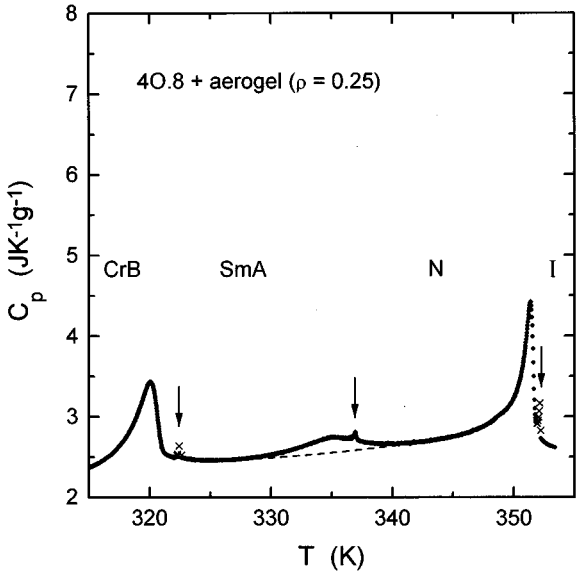

FIG. 4. Heat capacity obtained at $\omega_o/2$ for 4O.8 in a $\rho=0.25$ aerogel. The spikes marked by arrows are due to a small excess of bulk 4O.8 on the surface as discussed in the text. As in Figs. 1 and 2, $\times$ symbols denote artificial C_p values obtained in two-phase coexistence regions where the phase shift ϕ is anomalous.

starting material. No shift was observed for T_{NA} or T_{AB} and the shift for T_{NI} was only -50 mK.

In the case of the one 4O.8+phobic aerosil sample with $\rho_s=0.109$ g cm^{-3} (heat capacity not shown), there is a greater rounding of all the C_p peaks than for the comparable philic sil sample. Furthermore, the SmA–CrB C_p peak and tanϕ peak are doubled, each showing two first-order components about 0.66 K apart. A full discussion of the behavior of LC+phobic sil samples, especially at first-order transitions, will be given elsewhere in the context of a 7O.4+aerosil study [23].

The heat capacity of 4O.8 confined in an aerogel of density 0.25 g cm^{-3} is given in Fig. 4. In this system each broad transition peak is accompanied by a small sharp spike at slightly higher temperatures. The same qualitative sort of behavior has been observed for 8CB in aerogels with densities 0.08–0.60 g cm^{-3}, where the spikes were due to excess bulk 8CB on the surface of the aerogel and the temperatures of the spikes coincided with the bulk LC transition temperatures [5]. The same is true for this 4O.8+aerogel sample. Not only do the three C_p spikes marked by arrows in Fig. 4 lie at the same temperatures as the bulk N-I, N–SmA, and SmA–CrB transitions, the phase-shift behavior is also consistent with a small amount of excess bulk 4O.8 on the surface. Both the N-I and SmA–CrB C_p spikes have associated sharp peaks in tan ϕ as expected for first-order features, and the N–SmA C_p spike is accompanied by a small but sharp dip in tanϕ. Thus these C_p spikes act as convenient internal markers of the bulk transition positions, and make it easy to determine the temperature shifts of transition features associated with 4O.8 in the pores of the aerogel. It should be noted that tanϕ associated with each rounded aerogel C_p peak exhibits a pronounced dip, which indicates a continuous transition. However, there are dynamics associated with the N-I and SmA–CrB transitions since there are broad peaks in C''_{filled} at both these transitions. This behavior is consistent with previous work on 4O.8 in more porous aerogels with densities $\rho=0.08$ and 0.17 g cm^{-3} [6], where the frequency dependence of C_p was measured in order to characterize the relaxation processes involved.

Table I summarizes several key features of our results: the shifts in transition temperatures relative to bulk 4O.8, the width of N-I and SmA–CrB coexistence regions, and the integrated enthalpies δH of the N–SmA and N-I peaks. In the latter case, the first-order latent heat ΔH is unknown so the total enthalpy $\delta H+\Delta H$ is undetermined for 4O.8+aerosil and 4O.8+aerogel samples. It is clear from Table I that the width of the nematic range varies only slightly. It is 15.16 K for bulk 4O.8, decreases monotonically

TABLE I. The shift in transition temperatures relative to bulk 4O.8 and the two-phase coexistence widths at first-order N-I and SmA–CrB(AB) transitions for 4O.8+aerosils of density ρ_s in g cm^{-3} and 4O.8 in an aerogel of density 0.25 g cm^{-3}. Also given are the integrated enthalpies δH for N–SmA(NA) and N-I transitions. All temperature shifts and coexistence widths are in K. The δH values are in J per gram of liquid crystal. In the case of the strongly first-order SmA–CrB transition, shifts were determined with respect to the position of the abrupt rise in C_p on cooling. For bulk 4O.8 $T_{NI}=352.081$ K (center of coexistence region), $T_{NA}=336.924$ K, $T_{AB}=322.37$ K (center of coexistence region) and 322.714 K (point of abrupt rise in C_p on cooling). For the aerogel with empty gel density 0.25 g cm^{-3}, the value $\rho_s=(\text{gel})/\phi_p$ is used; see text.

Sample	ρ_s	ΔT_{NI}	NI coex.	ΔT_{NA}	ΔT_{AB}	AB coex.	δH_{NA}	δH_{NI}
bulk	0	0	0.27	0	0	0.68	2.18[a]	6.87[b]
sil(philic)	0.028	−1.69	0.32	−1.66	−1.68	1.28	1.95	7.15
	0.051	−2.05	0.35	−1.75	−1.62	1.07	1.88	6.74
	0.109	−2.19	0.27	−1.79	−1.29	1.38	1.73	7.52
	0.231	−3.44	0.27	−2.86	−2.19	1.23	1.41	6.58
	0.438	−5.77	∼0.4	−4.47	−3.36	∼1.3	1.28	6.72
sil(phobic)	0.109	−1.38	∼0.4	−2.30	−1.60[c]	∼2.0	1.19	7.02
					−2.26			
gel	0.29	−0.72		−1.64	−2.65		1.13	5.58

[a]This value agrees well with 2.11 in Ref. [16] and 2.19 in Ref. [6].

[b]The total N-I enthalpy $\Delta H+\delta H$ is 7.66 J g^{-1} [6].

[c]There are two entries here since the C_p(SmA–CrB) peak is doubled in the presence of a phobic sil.

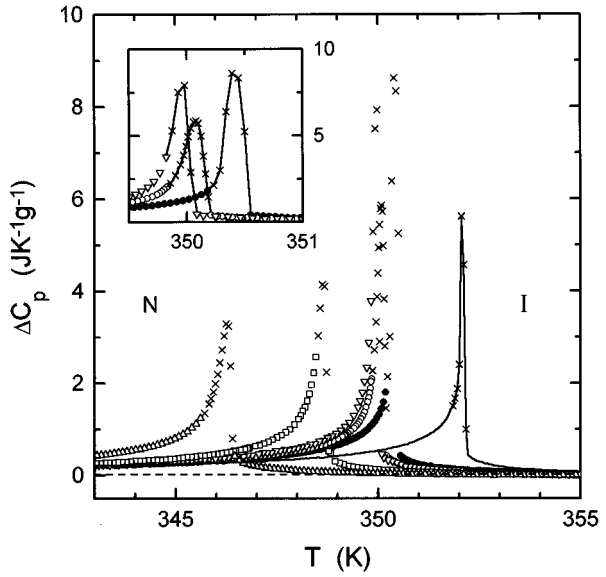

FIG. 5. Overlay of excess heat capacity $\Delta C_p(N\text{-}I)$ for bulk 4O.8 (solid line) and 4O.8+philic aerosil samples with $\rho_s=0.028$ (●), 0.051 (○), 0.109 (▽), 0.231 (□), and 0.438 (△). In all cases, data in two-phase coexistence regions are marked by ×. For clarity, only half the observed points are shown. The inset shows a detailed view near C_p(max) for $\rho_s=0.028$, 0.051, and 0.109 sils.

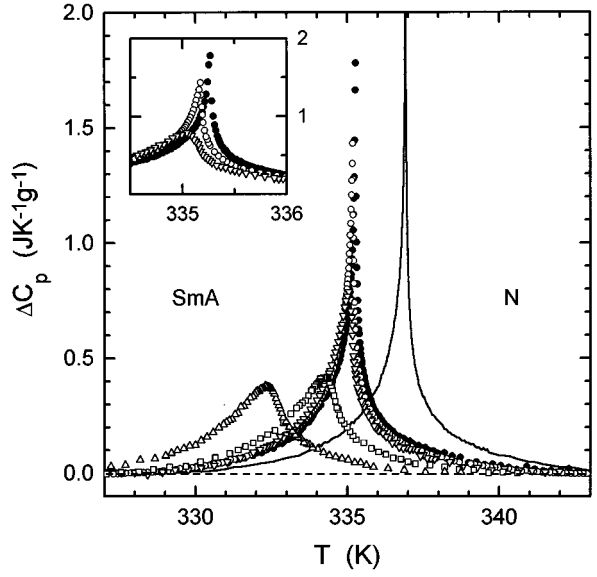

FIG. 6. Overlay of excess heat capacity $\Delta C_p(N-\mathrm{Sm}A)$ for bulk 4O.8 (solid line) and 4O.8+philic aerosil samples (symbols the same as in Fig. 5). For clarity, only one-tenth of the observed points are shown. The inset shows a detailed view near C_p(max) for $\rho_s=0.028$, 0.051, and 0.109 sils.

in the philic sil samples to 13.86 K for $\rho_s=0.438$ g cm^{-3}, is 16.08 K in the only phobic sil sample, and is 16.07 K for the gel sample.

III. ANALYSIS

It will be helpful for comparing the phase transition behavior of various samples to generate excess heat capacity curves:

$$\Delta C_p = C_p - C_p(\text{background}). \tag{3}$$

In the case of $\Delta C_p(N-\mathrm{Sm}A)$, the C_p(background) curve represents the trend in C_p that would be expected in the low-temperature tail of the N-I peak if no SmA phase were to form (see Ref. [5]). This background is given by the dashed lines in the $N-\mathrm{Sm}A$ region of Figs. 1, 2, and 4. In the case of $\Delta C_p(N\text{-}I)$, the C_p(background) line is almost horizontal like the dashed-dot line shown in Fig. 1. The resulting $\Delta C_p(N\text{-}I)$ and $\Delta C_p(N-\mathrm{Sm}A)$ curves are given in Figs. 5 and 6. Since the transition temperatures for sil samples with $\rho_s=0.028$, 0.051, and 0.109 g cm^{-3} are close together, an inset of the C_p peak region on an expanded T scale has been included for these three samples.

The Sm$A-$CrB transition is strongly first order; $\Delta H_{AB} \simeq 8\ \delta H_{NA}$ for bulk 4O.8 [6,16a]. Furthermore, there is a very wide two-phase coexistence region for 4O.8+philic sils and the phobic sil sample exhibits a doubled Sm$A-$CrB peak, as shown in Table I. Thus, most of the C_p points in the Sm$A-$CrB peak region are artificial values distorted by latent heat effects, and the quantity $\Delta C_p(\mathrm{Sm}A-\mathrm{Cr}B)$ is of little or no value.

N-SmA power-law fits. Since the $N-\mathrm{Sm}A$ heat-capacity peak is very sharp for philic sil samples with $\rho_s=0.028$ and 0.051, and still fairly sharp even for the $\rho_s=0.109$ philic sample, a power-law critical analysis has been carried out using the usual form including correction terms [24]

$$\Delta C_p = A^{\pm}|t|^{-\alpha}(1+D_1^{\pm}|t|^{0.5}+D_2^{\pm}|t|)+B_c, \tag{4}$$

where $t\equiv(T-T_c)/T_c$ is the reduced temperature and B_c is the contribution of the singular free energy to the regular heat capacity. For least-squares fits with Eq. (4), we used $t_{\min}^{+}=+10^{-4}$ and the $t_{\min}^{-}$ values given in Table II. Thus a small region is deleted near T_c where rounding effects occur in the sil samples, and also where systematic deviations were observed for bulk 4O.8. The fitting parameters given in Table II were obtained with $|t|_{\max}=6\times10^{-3}$, but the parameter stability was tested by range shrinking techniques with $|t|_{\max}=3\times10^{-3}$ and 10^{-2}.

The fits for bulk 4O.8 ($\rho_s=0$) are in good agreement with those reported in Refs. [6] and [17]. α and A^-/A^+ values of 0.133 and 1.243 were reported in Ref. [6], and 0.134 $\pm$0.015 and 1.132$\pm$0.16 were reported in Ref. [17]. As the sil density ρ_s is increased, the effective exponent α decreases smoothly from 0.135 to $\sim$0. The 95% confidence limits on these α values are rather broad due to the gap near T_c. However, the stability of free α values for the three fitting ranges is good, as shown in the last column of Table II. Moreover, the ratio A^-/A^+ was stable on range shrinking for the $\rho_s=0.028$ and $\rho_s=0.051$ sil samples, although not so stable for the $\rho_s=0.109$ sample. The overall trend in α_{eff} values is shown in Fig. 7. It should be noted that previous power-law fits to $\Delta C_p(NA)$ for bulk 4O.8 [6,17] and for 8CB+aerosil samples [11] were achieved with $D_2^{\pm}\equiv0$. Such fits were also carried out for the present data but did not yield very satisfactory results. If $D_2^{\pm}$ was held fixed at zero, all the fitting parameters, including the critical exponent α, were less stable to range shrinking than the fits given in

TABLE II. Results of fitting 4O.8+philic aerosil ΔC_p data with Eq. (4) over the range $|t|_{\max}=6\times10^{-3}$ (~600 points). Quantities in brackets were held fixed. The error bounds for $\alpha_{\rm eff}$ are 95% confidence limits determined by varying α through a series of fixed values and using the F test. The range of free $\alpha_{\rm eff}$ values obtained with fitting ranges $|t|_{\max}=3\times10^{-3}$ (~450 points) and $|t|_{\max}=10^{-2}$ (~750 points) is given as $\Delta\alpha$ in the last column. The sil density ρ_s is in g cm^{-3} units; the units of A^+ and B_c are J K^{-1} g^{-1}. $t^-_{\rm min}$ is the minimum t value used for data below T_c.

ρ_s	α	T_c (K)	A^+	A^-/A^+	D_1^+	D_1^-/D_1^+	D_2^+	D_2^-/D_2^+	B_c	χ^2_ν	$10^4 t^-_{\rm min}$	$\Delta\alpha$
0	0.135 ±0.09	336.924	0.876	1.212	3.673	0.047	−8.27	−0.60	−2.02	1.02	−3.2	0.129–0.139
0.028	0.064 ±0.09	335.269	2.736	1.105	1.822	0.058	−5.01	−0.32	−4.10	0.98	−1.5	0.054–0.064
0.051	0.039 ±0.08	335.173	4.917	1.080	0.981	−0.410	−2.69	−1.41	−6.25	1.02	−4.7	0.037–0.069
	[−0.007]	335.172	−43.26	0.987	−0.214	−0.176	0.729	−0.831	41.33	1.08	−4.7	
0.109	−0.066 ±0.16	335.133	−2.565	0.604	1.345	10.68	−12.02	6.67	1.986	0.92	−7.7	−0.004–(−0.066)
	[−0.007]	335.134	−11.88	0.947	0.425	3.248	−2.705	2.519	11.45	0.92	−7.7	

Table II. For the samples with $\rho_s=0.051$ and 0.109, the χ^2_ν values were significantly larger so that the $D_2^\pm\neq0$ fits in Table II are statistically better at the 95% confidence level. The pattern of decreasing α values with increasing ρ_s is less clear than for the fits with $D_2^\pm\neq0$, but $\alpha_{\rm eff}$ values from $D_2^\pm\equiv0$ fits all lie within the error bounds listed in Table II, and the general trend in α values is qualitatively the same. The reason that second correction-to-scaling terms play a more prominent role for the present data is unclear.

Although the change in the width of the N range of sil samples is quite insignificant and this is the factor controlling the crossover related to smectic-ψ–nematic-S coupling in bulk LC's, one sees crossover in Fig. 7 from $\alpha_{\rm eff}=0.135$ in the bulk to $\alpha_{\rm eff}\simeq\alpha_{XY}$ in 4O.8+sil samples with $\rho_s\simeq0.08$ g cm^{-3}. For samples with ρ_s greater than an estimated 0.09 g cm^{-3}, gel-like rounding of the peak is progressively obvious as ρ_s increases. Note for $\rho_s=0.109$ g cm^{-3} that the magnitude of $t^-_{\rm min}$ has increased considerably (rounding is more pronounced below T_c than above), the ratios of fitting parameters A^-/A^+, D_1^-/D_1^+, and D_2^-/D_2^+ are all quite different from the other samples listed in Table II, and these parameters themselves are fairly unstable on range shrinking. We consider the $\rho_s=0.109$ sample to be just beyond the density limit where quasi-singular C_p peaks occur, and the fit to this sample is less certain in spite of good χ^2_ν values. The choice of ~0.09 g cm^{-3} as the density limit of sharp singular $C_p(N-{\rm Sm}A)$ peaks is consistent with the clearly rounded $N-{\rm Sm}A$ peak observed in the 4O.8+phobic sil with $\rho_s=0.109$ g cm^{-3}.

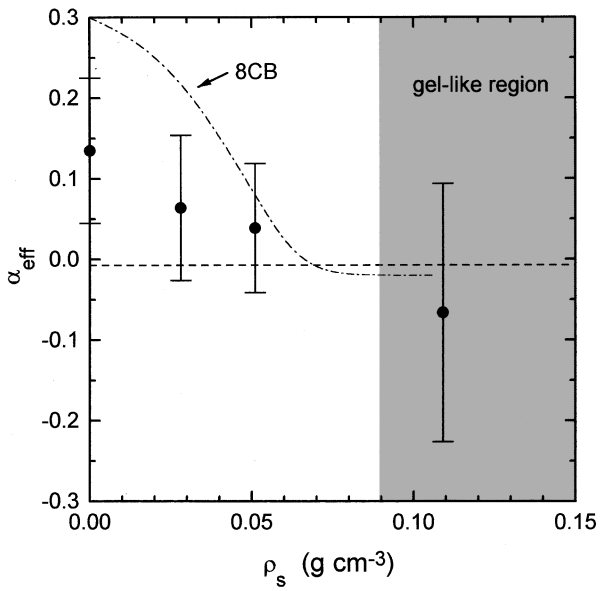

FIG. 7. Critical $N-{\rm Sm}A$ heat-capacity exponent $\alpha_{\rm eff}$ as a function of ρ_s for 7O.4+philic aerosil samples. The dashed horizontal line indicates the value of α_{XY}. The dot-dashed line indicates the smooth curve variation of $\alpha_{\rm eff}$ for 8CB+aerosils [11]. For ρ_s values greater than ~0.09 g cm^{-3} the $N-{\rm Sm}A$ peak is rounded in the same way as in aerogel samples.

IV. DISCUSSION

The phase transition temperatures for bulk 4O.8 and 4O.8+philic aerosil samples are given as a function of ρ_s in Fig. 8. Note that for all three transitions investigated, there is a very substantial decrease in the transition temperature T_t relative to the bulk value for $\rho_s=0.028$, and then an effective plateau in T_t values out to $\rho_s\simeq0.1$, beyond which T_t falls linearly. Roughly the same behavior is observed for 8CB+aerosils, but the size of the T_t shifts are smaller for 8CB by a factor of about 2 [11,25]. Such a difference is presumably related to the fact that 4O.8 can hydrogen bond to the hydroxyl groups on a philic surface whereas 8CB cannot, making the surface perturbation in 4O.8 greater than that in 8CB.

In view of the quite substantial shifts in transition temperatures observed at very low silica densities, some long-range force must be involved, like orientational elastic effects. If elastic effects (say bend and splay in the nematic region for example) play a major role in introducing defects and dislocations into the liquid crystal due to effects of the surface, any ordering must be influenced by such elastic defects. A detailed discussion of elastic perturbation effects will be given elsewhere [25].

A. N-I transition

The N-I transition in bulk 4O.8 has a substantial latent heat ($\Delta H\simeq3.36$ J g^{-1}) as well as integrated enthalpy in the

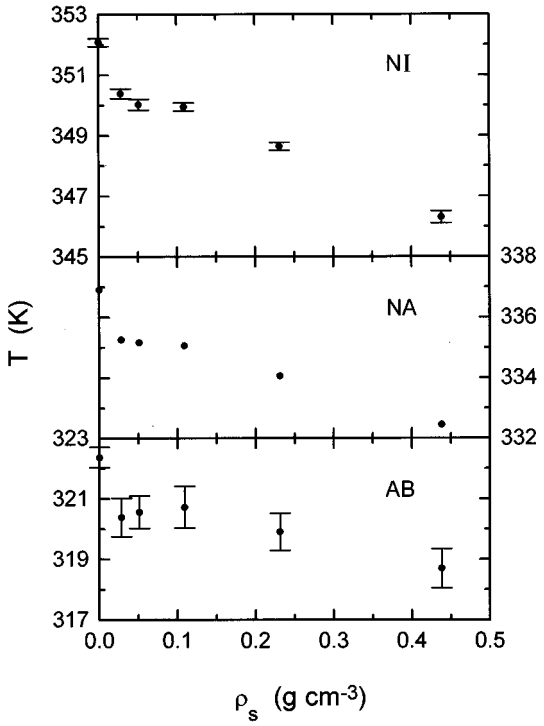

FIG. 8. Dependence of the transition temperatures $T_1(N\text{-}I)$, $T_c(N-\mathrm{Sm}A)$, and $T_1(\mathrm{Sm}A-\mathrm{Cr}B)$ on the silica density ρ_s for 4O.8+philic aerosil systems. For $N\text{-}I$ and SmA–CrB transitions, the vertical bars show the widths of the two-phase coexistence regions, and the points are located at the center of these regions.

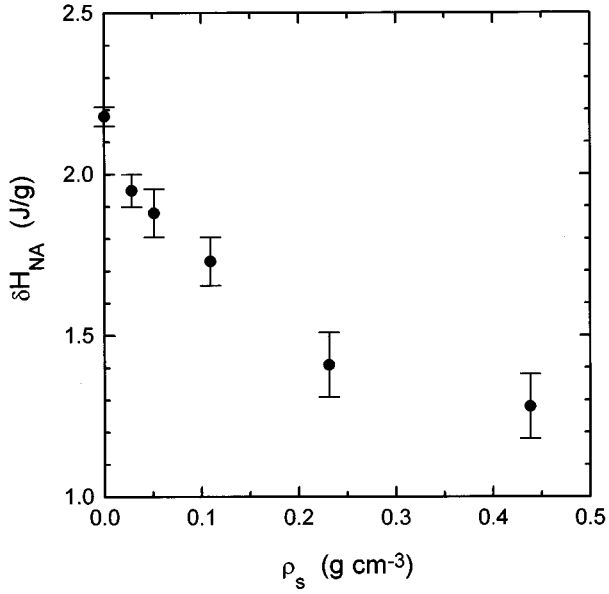

FIG. 9. Variation of the integrated $N-\mathrm{Sm}A$ enthalpy δH_{NA} with ρ_s for 4O.8+philic aerosil samples. The error bars represent the estimated uncertainty due to the choice of C_p(background).

wings ($\sim$4.30 J g^{-1}) [6]. The δH_{NI} bulk value in Table I of 6.87 J g^{-1} clearly includes some of this latent heat contribution. The same is presumably true of all the investigated sil samples since they all exhibit weak first-order behavior. Studies of 8CB+aerosil or aerogel samples indicate that for 8CB the $N\text{-}I$ transition is first order in sils for $\rho_s \leqslant 0.167$ g cm^{-3} and in a $\rho=0.17$ gel, but becomes continuous in a $\rho=0.36$ gel. Note that the comparable density ρ_s for a gel is $\rho(\mathrm{gel})/\phi_p=0.19$ for a $\rho=0.17$ gel and 0.455 for a $\rho=0.36$ gel [5,11]. The continuous $N\text{-}I$ transition for 4O.8 in a gel characterized by $\rho_s \simeq 0.29$ fits into this pattern of behavior for aerogel perturbed LC's.

The qualitative trend in the shape of $\Delta C_p(NI)$ sil peaks and their temperature shift from bulk are visible in Fig. 5. A plot of $T_1(NI)$ vs ρ_s is given in Fig. 8. One feature in the $N\text{-}I$ region that is not visible from Fig. 5 is a tiny subsidiary C_p peak located above the temperature of the major $N\text{-}I$ peak. For the $\rho_s=0.231$ sample, this secondary peak was $\sim$0.20 K above the main peak and was narrow ($\sim$50-mK full width) and small ($\delta H \simeq 5$ mJ g^{-1}); it was only visible for slow scans at lower frequencies ($\omega_o/2$ or $\omega_o/5$). For the $\rho_s=0.051$ sample, the shift was $\sim$0.09 K, and this feature appears only as a shoulder on the high-temperature side of the $N\text{-}I$ peak. Very conspicuous doubling of the $N\text{-}I$ peak on adding aerosils has been observed for 8CB [11,25] and 7O.4 [23], and this is discussed in Ref. [25].

B. $N-\mathrm{Sm}A$ transition

The shifts in T_{peak} (the position of the C_p maximum) for 4O.8 samples with added philic aerosil are visible from Fig. 6, and the T_{peak} values are plotted versus ρ_s in Fig. 8. The trend in δH_{NA} values with ρ_s, shown in Fig. 9, exhibits a smooth variation, which is in qualitative agreement with 8CB+aerosil results [11]. There are, however, interesting differences between the behavior of 4O.8 and 8CB in aerogel and aerosil samples. For 8CB, the variations of T_{NA} and δH_{NA} superimpose for sils and gels. But, in the case of 4O.8, the T_{peak} shift for the aerogel is less than that for comparable sils and the δH_{NA} value is smaller. At present, we have no explanation for this difference in the behavior of 8CB and 4O.8 perturbed systems.

Finally, we should stress that the crossover of low-density 4O.8 aerosils to a XY-like value around $\rho_s \simeq 0.08$ g cm^{-3} is exactly parallel to a larger crossover from $\alpha_{\mathrm{eff}} \simeq 0.30 \pm 0.02$ for bulk 8CB to $\alpha_{\mathrm{eff}} \simeq \alpha_{XY}$ for a $\rho=0.084$ 8CB+aerosil sample [11], as shown in Fig. 7. The reason for such crossover appears to be that the aerosil reduces the nematic orientational susceptibility and changes the nature of the coupling between nematic-S and smectic-ψ order parameters. This idea is further supported by the fact that bulk 8S5 (octylphenylthiol-pentyloxybenzoate) has a critical exponent $\alpha \approx \alpha_{XY} = -0.007$ and a 8S5+aerosil sample with $\rho_s \simeq 0.08$ g cm^{-3} has an effective exponent $\alpha_{\mathrm{eff}} = -0.019 \pm 0.05 \approx \alpha_{XY}$ [11]. Thus the aerosil does not influence the character of the critical enthalpy fluctuations if ψ-S coupling is already unimportant in the bulk LC.

C. SmA–CrB transition

Not much can be said about the strongly first-order SmA–CrB freezing transition. The aerosil does not convert this transition or the more weakly first order $N\text{-}I$ transition into a continuous transition as predicted in general for all first-order transitions by a quenched random-field model [26]. This may be due to (a) deficiencies in the model, (b) inapplicability of the model since LC+aerosils are not completely quenched random systems (but note that

LC+aerogels also exhibit first-order transitions), (c) the effect is too weak to eliminate two-phase coexistence for such a strongly first-order transition. In connection with the latter point it should be noted from Fig. 2 that as the aerosil density increases, the extent of the one-phase Cr*B* pretransitional wing below the Sm*A*–Cr*B* coexistence range increases. In all systems studied, there are small but distinct pretransitional C_p wings both above and below the transition temperature.

D. 4O.8+aerogel behavior

Although the principal focus of the present investigation is on 4O.8+dispersed aerosil particles, a few concluding remarks are appropriate about the similarities and differences of the behavior of the present 4O.8+aerogel sample from the behavior of other LC+aerogel systems. The overall transition behavior of 4O.8 in a $\rho=0.25$ aerogel is very close to that for 8CB in a $\rho=0.17$ aerogel. In both cases, there are small sharp C_p spikes that lie exactly at the temperatures of bulk LC transitions and arise from a small quantity of unperturbed excess bulk on the external surface of the gel. Furthermore, the temperature shifts of the aerogel *N*-*I* and *N*–Sm*A* transitions are almost the same. The 8CB shifts in a $\rho=0.17$ gel are $\Delta T_{NI}=-0.72\pm0.05$ K and $\Delta T_{NA}=-1.62\pm0.10$ K [5], and the corresponding shifts in Table I for 4O.8 in a $\rho=0.25$ gel are -0.724 and -1.64 K.

There are puzzling disagreements between the present 4O.8+aerogels results and previously reported work on 4O.8 in $\rho=0.08$ and 0.17 aerogels [6]. In the earlier investigation, both the sharp C_p spikes and the broad LC+aerogel peaks were shifted by large amounts from the positions of bulk transitions (3–5 K in the case of *N*-*I* and *N*–Sm*A* features). The cause of such large shifts is not clear. Possibly there were substantial drifts toward lower temperatures during very long runs that were due to thermal generation of impurities rather than aerogel perturbations, but that is highly speculative. In any event, there are two strong similarities between the present 4O.8+aerogel data and the previous 4O.8+aerogel results for a gel with $\rho=0.17$ [6]. The size and shapes of the broad C_p peaks in Fig. 4 are very close to those given in Fig. 2 of Ref. [6]. Furthermore, the shifts between the rounded aerogel C_p peaks and the sharp C_p spikes agree well. For Ref. [6], the differences T_t(aerogel)$-T_t$(spike) were -0.9 K for *N*-*I*, approximately -1.7 K for *N*–Sm*A*, and -2.4 K for Sm*A*–Cr*B*, which are close to the corresponding shifts in Table I.

For 7O.4 in aerogels with densities 0.08 and 0.17 g cm^{-3} [7], spikes due to excess LC on the surface were also seen. In this case, the temperatures of the *N*–Sm*A* and Sm*C*–Cr*G* spikes agreed well with those for bulk 7O.4 transitions. However, the *N*-*I* surface spike was 0.6 K lower and the Sm*A*–Sm*C* surface spike was 1.0 K lower than bulk 7O.4 transition temperatures, for reasons that are not clear.

ACKNOWLEDGMENTS

The authors wish to thank J. D. Litster for providing the 4O.8 sample, G. S. Iannacchione for experimental assistance, and both G. S. Iannacchione and Z. Kutnjak for helpful and stimulating discussions. This work was supported by NSF Grant No. DMR 93-11853.

[1] J. P. Hill, Q. Feng, Q. J. Harris, R. J. Birgeneau, A. P. Ramirez, and A. Cassanho, Phys. Rev. B **55**, 356 (1997), and references cited therein.
[2] T. Bellini *et al.*, Phys. Rev. Lett. **69**, 788 (1992).
[3] N. A. Clark *et al.*, Phys. Rev. Lett. **71**, 3050 (1993).
[4] T. Bellini, N. A. Clark, and D. W. Schaefer, Phys. Rev. Lett. **74**, 2740 (1995).
[5] L. Wu, B. Zhou, C. W. Garland, T. Bellini, and D. W. Schaefer, Phys. Rev. E **51**, 2157 (1995), and references cited therein.
[6] Z. Kutnjak and C. W. Garland, Phys. Rev. E **55**, 488 (1997).
[7] H. Haga and C. W. Garland, Liq. Cryst. **22**, 275 (1997).
[8] G. S. Iannacchione, S. Qian, D. Finotello, and F. Aliev, Phys. Rev. E **56**, 554 (1997).
[9] G. S. Iannacchione, G. P. Crawford, S. Zumer, J. W. Doane, and D. Finotello, Phys. Rev. Lett. **71**, 2595 (1993); Phys. Rev. E **53**, 2402 (1996).
[10] *Liquid Crystals in Complex Geometries Formed by Polymer and Porous Networks*, edited by G. P. Crawford and S. Zumer (Taylor and Francis, London, 1996), and references therein.
[11] B. Zhou, G. S. Iannacchione, C. W. Garland, and T. Bellini, Phys. Rev. E **55**, 2962 (1997).
[12] J. C. LeGuillon and J. Zinn-Justin, **39**, 95 (1977); Phys. Rev. B **21**, 3976 (1980); C. Bagnuls and C. Bervillier, Phys. Lett. A **112**, 9 (1985).
[13] C. W. Garland and G. Nounesis, Phys. Rev. E **49**, 2964 (1994).
[14] G. S. Iannacchione, J. Mang, and T. Rieker (private communication).
[15] S. Jen, N. A. Clark, and P. S. Pershan, J. Chem. Phys. **66**, 4635 (1977); J. W. Goodby, J. W. Gray, A. J. Leadbetter, and M. A. Mazid, in *Liquid Crystals of One- and Two-Dimensional Order*, edited by W. Halfrich and G. Heppke (Springer-Verlag, Berlin, 1980), p. 3; G. W. Smith, Z. G. Gardlund, and R. J. Curtis, Mol. Cryst. Liq. Cryst. **19**, 327 (1973); G. W. Smith and Z. G. Gardlund, J. Chem. Phys. **59**, 3214 (1973).
[16] (a) K. J. Lushington, G. B. Kasting and C. W. Garland, J. Phys. (France) Lett. **41**, L-419 (1980); R. J. Birgeneau, C. W. Garland, G. B. Kasting, and B. M. Ocko, Phys. Rev. A **24**, 2624 (1981).
[17] K. J. Stine and C. W. Garland, Phys. Rev. A **39**, 3148 (1989).
[18] Degussa Corp., Silica Division, 65 Challenger Rd., Ridgefield Park, NJ 07660.
[19] B. Zhou, G. S. Iannacchione, and C. W. Garland, Liq. Cryst. **22**, 335 (1997).
[20] C. W. Garland, Thermochim. Acta **88**, 127 (1985); *Liquid Crystals: Physical Properties and Phase Transitions*, edited by S. Kumar (Oxford University Press, New York, in press), Chap. 6.
[21] H. Yao, T. Chan, and C. W. Garland, Phys. Rev. E **51**, 4585 (1995).

[22] X. Wen, C. W. Garland, and M. D. Wand, Phys. Rev. A **42**, 6087 (1990).
[23] H. Haga and C. W. Garland, Liq. Cryst. (to be published).
[24] C. W. Garland, G. Nounesis, M. J. Young, and R. J. Birgeneau, Phys. Rev. E **47**, 1918 (1993).
[25] G. S. Iannacchione and C. W. Garland (unpublished).
[26] A. Falicov and A. N. Berker, Phys. Rev. Lett. **76**, 4380 (1996), and references cited therein.